



1 **Deposition of light-absorbing particles in glacier snow of the Sunderdhunga Valley, the**  
2 **southern forefront of Central Himalaya**

3

4 Jonas Svensson<sup>1,2</sup>, Johan Ström<sup>3</sup>, Henri Honkanen<sup>4</sup>, Eija Asmi<sup>1</sup>, Nathaniel B. Dkhar<sup>5</sup>, Shresth  
5 Tayal<sup>5,6</sup>, Ved P. Sharma<sup>5,6</sup>, Rakesh Hooda<sup>1</sup>, Matti Leppäranta<sup>4</sup>, Hans-Werner Jacobi<sup>2</sup>, Heikki  
6 Lihavainen<sup>7,1</sup>, Antti Hyvärinen<sup>1</sup>

7 1 Atmospheric Composition Research, Finnish Meteorological Institute, Helsinki, Finland

8 2 Université Grenoble Alpes, CNRS, IRD, INP-G, IGE, Grenoble, France

9 3 Department of Environmental Science, Stockholm University, Stockholm, Sweden

10 4 Institute for Atmospheric and Earth System Research, Faculty of Science, University of Helsinki,  
11 Helsinki, Finland

12 5 The Energy and Resource Institute, (TERI), New Delhi, India

13 6 TERI School of Advanced Studies (TERI SAS), New Delhi, India

14 7 Svalbard Integrated Arctic Earth Observing System, Longyearbyen, Norway

15

16 Correspondence to: jonas.svensson@fmi.fi

17

18 **Abstract**

19 Anthropogenic activities on the Indo-Gangetic Plain emit vast amounts of light-absorbing particles  
20 (LAP) into the atmosphere, modifying the atmospheric radiation scheme. With transport to the nearby  
21 Himalayan mountains and deposition to its surfaces the particles contribute to glacier and snowmelt via  
22 darkening of the highly reflective snow. The Central Himalayas have been identified as a region where  
23 LAP are especially pronounced in glacier snow, but still remain a region where measurements of LAP  
24 in the snow are scarce. Here we study the deposition of LAP in five snow pits sampled in 2016 (and  
25 one from 2015) from two glaciers in the Sunderdhunga valley, state of Uttarakhand, India, Central  
26 Himalaya. The snow pits display a distinct melt layer interleaved by younger snow above, and older  
27 snow below. The LAP exhibit a distinct vertical distribution in these different snow layers. For the  
28 analyzed elemental carbon (EC), the younger snow layers in the different pits show similarities, and  
29 can be characterized by a deposition constant of about  $50 \mu\text{g m}^{-2} \text{mm}^{-1}$  while the old snow layers also  
30 indicate similar values, and can be described with a deposition constant of roughly  $150 \mu\text{g m}^{-2} \text{mm}^{-1}$ .  
31 The melt layer, contrarily, display no similar trends between the pits. Instead, it is characterized by very  
32 high amounts of LAP, and differ in orders of magnitude for concentration between the pits. The melt  
33 layer is likely a result of strong melting that took place during the summers of 2015 and 2016. The  
34 mineral dust fractional absorption is slightly below 50 % for the young and old snow layer, whereas in  
35 the melt layer is the dominating light absorbing constituent, thus, highlighting the importance of dust



36 in the region. Our results indicate the problems with complex topography in the Himalaya, but  
37 nonetheless, can be useful in large-scale assessments of LAP in Himalayan snow.



## 38 1 Introduction

39 Aerosol particles in the Indo-Gangetic Plain (IGP) are produced in great mass and number. Being  
40 especially prominent in the pre-monsoon season, a large fraction of the airborne aerosols are  
41 carbonaceous particles, consisting of organic carbon (OC) and black carbon (BC). Originating from the  
42 combustion of fossil fuels and biomass, the particles form the atmospheric brown cloud—known to  
43 modify the atmospheric radiation scheme (Lau et al., 2006; Menon et al., 2010; Ramanathan and  
44 Carmichael, 2008). Through air mass transport the aerosol can be conveyed and lifted from the IGP to  
45 its northern barrier, the mountains of Himalaya (e.g. Hooda et al., 2018; Kopacz et al., 2011;  
46 Raatikainen et al., 2014; Zhang et al., 2015). Covered with vast amounts of snow and ice, the Himalayan  
47 cryosphere is affected by the deposition of carbonaceous aerosol onto its surface (e.g. He et al., 2018;  
48 Jacobi et al., 2015; Ménéguez et al., 2014; Xu et al., 2009). This is due to the particulates and especially  
49 BC effectiveness in reducing the snow albedo (Warren and Wiscombe, 1980), which ultimately leads  
50 to accelerated snow melt (Flanner et al., 2007; Jacobi et al., 2015; Jacobson, 2004; Ming et al., 2012).

51

52 In addition to BC and OC, other particles such as mineral dust (MD) and snow microbes (collectively  
53 known as light-absorbing particles (LAP)) are also of importance in reducing snow albedo (e.g. Skiles  
54 et al. 2018). In Himalayan snow and ice, the LAP content has been shown to vary significantly, both  
55 spatially and temporally (e.g. see review by Gertler et al., 2016). Further, an extensive compilation of  
56 BC measurements in snow over the Tibetan Plateau is presented in the supplement of He et al. (2018),  
57 with concentrations ranging from 1 to 3600 ppb in the region termed as Himalaya. In addition to long  
58 range transported LAP, local sources within the Tibetan plateau have also been documented to be  
59 significant in some regions (e.g. Li et al., 2016), creating several different sources of LAP in the snow.  
60 Varying meteorology and terrain induced exchange processes (advection and turbulence) in the  
61 mountains further complicates the interplay between the atmospheric deposition of LAP and the snow  
62 surfaces.

63

64 Observations are further supported by modeling studies, which indicate certain sub-regions of the  
65 Himalaya to be especially vulnerable to LAP deposition. Santra et al. (2019) recently simulated the BC  
66 impact on snow albedo and glacier runoff in the Hindu Kush-Himalaya region. The authors identified  
67 a hot-spot zone for BC in the vicinity of Manora peak, located in the Indian state of Uttarakhand, central  
68 Himalaya (also sometimes called western Himalaya depending on classification). The BC induced a  
69 greater albedo reduction on glacier snow in the vicinity of this hot spot area compared to other areas in  
70 the Hindu Kush-Himalayan area. Similarly, another modeling study simulated the impact of LAP on  
71 High Mountain Asia snow albedo and its associated forcing and identified the same general area as a  
72 region where snow is especially affected by LAP-caused snow darkening (Sarangi et al., 2019). Both



73 of these studies (as well as the work of He et al., 2018) emphasized the need for more *in situ*  
74 measurements of LAP in the snow of this region of the Himalaya.

75

76 Previously, we reported in Svensson et al. (2018) the measured LAP concentrations and properties in  
77 the snow from two glaciers in the Sunderdhunga valley, located in Uttarakhand, India, central Himalaya.  
78 While we mainly focused on the surface snow layer and characterizing the LAP, results from one 1.2  
79 m deep snow pit were also presented. Based on the LAP concentration profile and pit stratigraphy, the  
80 pit was estimated to represent 5 seasons. Newly sampled snow pits have since then been analyzed from  
81 the same two glaciers, along with available automatic weather station (AWS) data from the same valley.  
82 Here we revisit the previous interpretation of the published pit (in Svensson et al., 2018), and report the  
83 results of our newly sampled snow pits. By comparing the BC profiles among 6 pits we aim at  
84 quantifying the deposition of elemental carbon (EC; used here as a proxy for BC) in this area of the  
85 Himalaya. In addition, we explore the relative contribution of MD to LAP in the different pits.

86

## 87 2 Methodology

### 88 2.1 Glaciers snow sampling and filtration

89 Snow was collected on Bhanolti and Durga Kot glaciers during a field campaign in the Sunderdhunga  
90 valley (located in the Bageshwar district) in October of 2016. The two glaciers are positioned adjacent  
91 to each other in a general northeast-southwest orientation (cf. Fig. 1) on the southern fringe of the  
92 Himalayan mountain range and are further described in Svensson et al. (2018). Local emissions of  
93 carbonaceous aerosol in the Sunderdhunga valley are very limited. The valley is not accessible by car  
94 and the glaciers are at a three to four-day hike from the nearest road. On route to the glaciers the last  
95 settlement is Jatoli, located in a river valley at an elevation of 2400 m. a.s.l. about 10 km southeast in a  
96 perpendicular orientation to the glacier valley. Biomass burning is a common practice for cooking and  
97 heating in Jatoli, thus some emissions from the village may enter the glacier valley. It is expected,  
98 however, that the majority of carbonaceous particles in the glacier valley originates from regional and  
99 long-distance transport. The relatively low elevation span as well as the glaciers' position on the  
100 southern slopes of the Himalayan mountains nonetheless, make them more prone to LAP deposition  
101 compared to other glaciers in the Himalaya and Tibetan plateau. Previous studies have reported elevated  
102 LAP content in lower elevation snow for Himalayan glaciers (e.g. Ming et al., 2013), and higher  
103 concentrations of LAPs in glaciers on the southern edge of the Himalaya (e.g. Xu et al., 2009).

104

105 On Durga Kot glacier two snow pits (hereafter Pit A and B; Fig. 1) were dug in the vicinity of each  
106 other (~20 m) in an reachable area of the percolation zone of the glacier. Bhanolti glacier was more  
107 easily accessible, and the three excavated snow pits (hereafter Pit C, D, E; Fig. 1) were spread out over  
108 a greater distance (~500 m) on the glacier (see table 1 and Fig. 1 for additional information). The depth



109 of the pits depended on the level at which a hard layer was found, and digging could not be further  
110 conducted. The deepest snow pit that was analyzed previously in Svensson et al. (2018), referred to as  
111 pit 5 in that study, is from Bhanolti glacier in September of 2015, and we denote as Pit F in the  
112 subsequent sections of this manuscript. As for the other pits from 2016, the depth of Pit F was governed  
113 by the depth at which the hard layer was encountered.

114

115 Three distinctly different colored snow layers could be observed repeating in all but one of the year  
116 2016 pits: a relatively thin (on the order of centimeters) very dark layer was separated by white snow  
117 above and more grey appearing snow below. Due to this stratigraphy, we hereafter simply refer to the  
118 whitest snow as young snow, the darkest layer as the melt layer, and the grey snow as old snow.  
119 Representative samples ranging from 3 to 10 cm thick layers were taken throughout each pit for analysis  
120 of LAP. Snow density measurements were conducted with a snow density kit in the upper part of the  
121 pits (in 5 cm increments) by weighing the known volume of the sampler filled with snow. The observed  
122 densities ranged between 0.29 and 0.46 g cm<sup>-3</sup> (see table 1 for details). Density measurements were not  
123 possible below the melt layer due to the hard snow. For these layers the density was assumed 0.5 g cm<sup>-3</sup>  
124 (to represent aged snow) in our further analyzes. Snow density measurements were not conducted for  
125 Pit F, and we assigned a density of 0.35 g cm<sup>-3</sup> for the top layer (0-3 cm; similar to observations made  
126 in 2016), followed by 0.4 g cm<sup>-3</sup> between 3-10 cm depth, and 0.5 g cm<sup>-3</sup> for all layers below 10 cm.  
127 Since the snow samples could not be transported in a solid phase back to the laboratory, they were  
128 melted and filtered at the nearby base camp using the same principles as in Svensson et al. (2018).  
129 Filters were transported back to the analysis laboratory in petri slides.

130

## 131 2.2 Meteorological observations

132 In September 2015 an AWS was installed next to the glacier ablation zone of Durga Kot (Fig. 1) about  
133 1.5 km northwards at an elevation below the snow sampling sites. The AWS is equipped with  
134 instruments for air temperature, relative humidity, shortwave (SW) and longwave (LW) radiation (up  
135 and down), wind speed and direction, and snow depth (Campbell Scientific SR50 Ultrasonic Distance  
136 Sensor). In this paper we use the snow depth data between September 2015 and September 2017 to  
137 estimate the local precipitation. The original snow depth data, logged once every 10 minutes was filtered  
138 to daily resolution by applying a moving median window of 24 hours and for the noon value of each  
139 day in further analyzes. This filtering removed much of the signal noise. However, before this filtering  
140 was applied the data was reduced using several logical conditions such as: the incoming SW radiation  
141 is greater than outgoing SW radiation (to remove errors due to sensors covered by snow), and the surface  
142 albedo is greater than 0.2 (to ensure snow cover). Finally, the consistency between the daily albedo and  
143 snow depth was inspected using data presented in Figure S1a. Each day the snow depth increased was  
144 interpreted as precipitation, and to arrive at an estimate of the snow water equivalent (SWE), the fresh



145 snow density is assumed to be  $100 \text{ kg m}^{-3}$ . The solid precipitation derived based on the cumulative SWE  
146 is presented in Figure S1b.

147

### 148 2.3 Filter analysis

149 The analysis of filters followed the procedure in Svensson et al. (2018), with transmission  
150 measurements coupled with thermal-optical analysis. According to the measurement nomenclature  
151 (Petzold et al., 2013), the carbonaceous constituents measured are EC and OC. The measurement  
152 method briefly follows the procedure of placing a filter punch in a custom-built particle soot absorption  
153 photometer (PSAP) to measure the transmittance (at  $\lambda = 526 \text{ nm}$ ; Krecl et al., 2007)—providing an  
154 optical depth for all of the particles captured by the filter. The filter punch is then placed in an OCEC  
155 analyzer (Sunset instrument, using the EUSAAR\_2 protocol) to determine the OC and EC mass,  
156 followed by another measurement with the PSAP. The OCEC analysis removes the carbonaceous  
157 species and, thus, by comparing the PSAP results obtained before and after the analysis, the relative  
158 contribution of the light absorption by EC particles in the total particles optical depth is obtained. The  
159 remaining optical depth we attribute as non-EC material. This fraction of the total optical thickness we  
160 report as the percentage of the mineral dust absorption on the filter samples (expressed as  $f_D$ ). For further  
161 details concerning the measurements see Svensson et al (2018).

162

163 Some of the filter samples ( $N=17$ ) were saturated with too much light absorbing material prohibiting  
164 reliable EC measurements despite reducing the sample to a melted equivalent of only 30 mL. To  
165 mitigate this problem, we calculated the EC indirectly from the analyzed total carbon (TC) for the  
166 saturated samples. From OCEC analysis TC is the most robust measured constituent, since it includes  
167 both OC and EC and is not affected by their split point, which may be incorrectly placed for very dark  
168 filters (Chow et al., 2001). A linear relation was fitted for non-saturated filter samples and the obtained  
169 correlation of  $EC = 0.10TC + 0.12$  was used to reconstruct the EC content for the filter samples  
170 containing high amounts of absorbing particles (see details in supplement and Fig. S3a-b). The slope  
171 compares well with the slopes reported for air samples collected at two sites in the Himalayas about  
172 550 km south-east from Sunderdhunga in the Kathmandu valley 32 km (altitude of 2150 m a.s.l.) east  
173 of Kathmandu, and Langtang 60 km north of Kathmandu (altitude of 3920 m a.s.l.) (Caricco et al., 2003).  
174 There, the authors found that the EC/TC ratio was 0.17 for both sites during the summer monsoon  
175 season, but between 0.10 and 0.13 during what they described as the ramp-up period and the peak  
176 concentration season. The snow samples do not have an upper limit for particles sizes, whereas the air  
177 samples were collected as PM<sub>2.5</sub> (particulate matter collected below an aerodynamic diameter of 2.5  
178  $\mu\text{m}$ ). The slopes are rather similar to our value, and the authors found as well a very strong correlation  
179 of 0.89 ( $r^2$ ) between monthly average EC and OC.

180



## 181 3 Results and discussion

### 182 3.1 EC deposition in young and old snow samples

183 When the EC content is analyzed from filtered snow samples, a common practice is to convert the  
184 results into mass concentrations [EC], given per volume or mass of melt water (e.g.  $\mu\text{g L}^{-1}$  or  $\text{ng g}^{-1}$ ).

185 A spread in results is often largely due to local processes and specific sampling layer thicknesses. The  
186 mass deposition per unit area  $\widehat{EC}$ , on the other hand, can be expected to be less variable with increasing  
187 number of layers used to calculate this value. The deposition in each layer is calculated according to:

188

$$189 \quad \widehat{EC}_i = [EC]_i \frac{\rho_{s_i}}{\rho_w} d_i \quad (1)$$

190

191 were  $\rho_s$  and  $\rho_w$  are snow and liquid water densities, respectively. The index  $i$ , is the number of the  
192 sampled layer from top to bottom, and  $\rho_s/\rho_w d$  is the SWE thickness,  $d_{SWE}$ . The  $\widehat{EC}_i$  and  $d_{SWEi}$  are  
193 transformed to cumulative plots by integrating over the layers from the surface to the bottom. These  
194 profiles are presented in Fig. 2a-f (with each sampling layer represented by a square).

195

196 The visible snow pit stratigraphy described above in section 2.1 can be observed in the pit profiles. At  
197 the top, the accumulated EC ( $EC_{acc}$ ) as a function of the accumulated  $d_{SWE}$  ( $SWE_{acc}$ ) portray the  
198 young snow layers, whereas in the bottom of the pits the data points represent the old snow layers (Fig.  
199 2a-f). This pattern (with both young and old snow layers) is visible in pits A, B, C, and D (Fig. 2a-d).  
200 These pits also have the melt layer interleaved between the young and old snow layers, indicated by the  
201 sharp increase (or steep slope) between the young and old snow layers. In the two pits where this general  
202 outline is not visible (pit E Fig. 2e and pit F Fig. 2f), it can be explained by the fact that pit E extended  
203 only to the melt layer (therefore no old snow samples) while pit F had essentially no young snow  
204 samples at the time of sampling (therefore pit F starts with the melt layer).

205

206 With the data points for young and old snow appearing rather similar in slope between the pits, the  
207 homogeneity is emphasized further by comparing the observations with common effective constants  
208 for young and old snow ( $EC_y^*$  and  $EC_o^*$ ), respectively. Suitable constants were determined to be close to  
209  $50 \mu\text{g m}^{-2}$  per mm SWE for young snow and  $150 \mu\text{g m}^{-2}$  per mm SWE for old snow (see supplement).  
210 The resulting deposition using  $EC_y^*$  and  $EC_o^*$  are superimposed over the observations in Figure 2a-e as  
211 dashed lines for young snow and dash-dotted lines for old snow. These lines then represent the constant  
212 deposition of EC as function of accumulated melt water in a column according to:

213

$$214 \quad EC_{acc} = constant * SWE_{acc} + offset \quad (2)$$

215



216 where  $EC_{acc}$  is the accumulated EC mass per  $m^2$  and  $SWE_{acc}$  is the accumulated melt water in  $L m^{-2}$   
217 (or mm), and the ‘constant’ is the deposition constant. The offsets for young snow are a result of  
218 enhanced observed EC concentration in the top layer, which can numerically be compensated for by  
219 “artificially” adding a small value to ( $\Delta SWE_{acc}$ ) to each pit, which in essence dilute the top layer, but  
220 have marginal effect on the overall picture. This meant simply rewriting the linear relation above into:  
221

$$222 \quad EC_{acc} = constant * (SWE_{acc} + \Delta SWE_{acc}) \quad (3)$$

223

224 The  $\Delta SWE_{acc}$  amounts were chosen by trial and error to be in multiples of 10 mm for simplicity. The  
225 resulting values were 10, 10, 60, 20, and 20 mm for pits A through E in order to explain the apparent  
226 offset. A physical interpretation of these numbers may be the loss of water from the surface layer due  
227 to evaporation or sublimation, which enhance  $[EC]$  in the top layer. For the old snow layers, snow and  
228 EC were numerically removed in the data by subtracting accumulated EC and SWE (including the melt  
229 layer, when present) down to the old snow layer. This was done such that the first data point satisfies  
230  $EC_o^*$ . Hence, for old snow  $[EC]_1 d_{SWE_1} / EC_o^* = SWE_{acc_1}$  where the index (1) represents the top layer of  
231 old snow.

232

233 By applying the offset values and numerically removing the upper snow layers, we compare the data in  
234 Fig. 2a-f in two separate figures (Fig. 3a-b), one where young snow are grouped together and one for  
235 old snow. In Fig 3a, the observed  $EC_{acc}$  is plotted against the  $EC_{acc}$  value if  $EC_y^*$  is used. In Fig. 3b  
236 the observed  $EC_{acc}$  is plotted against the  $EC_{acc}$  value if  $EC_o^*$  is used. Note that for old snow the first  
237 data point in the different pits will, by definition, be on the 1:1 line. Nevertheless, the consistency  
238 between the pits is striking and the fact that much of the variation in  $EC_{acc}$  as function of  $SWE_{acc}$  (or  
239 depth in the pit) can be explained by  $EC_y^*$  and  $EC_o^*$  alone is a very interesting finding.

240

### 241 3.2 Melt layer

242 On the contrary to the observed similarities in the different pits between young and old snow, the melt  
243 layer samples do not display similar trends. Instead of being characterized by a common constant, the  
244  $EC_{acc}$  value as function of  $SWE_{acc}$  in the melt layer differs by orders of magnitude between the  
245 different pit profiles. To explore the melt layers further, we make use of the constant for young snow,  
246  $EC_y^*$ . Assuming that this is a characteristic value for precipitation during the winter season, we can  
247 estimate the required amount of precipitation ( $SWE_{acc}$ ) that is needed to explain the observed  $EC_{acc}$   
248 deposition. These derived precipitation amounts for each pit are presented in Figure 4 as a function of  
249 the relative depth from the surface to the bottom of the pit. Using this approach, pit F corresponds to a  
250 total equivalent of about 2100 mm in precipitation, whereas pits B, E, and D represent 3500, 4300, and  
251 5100 mm, respectively. Pits A and C deviate starkly from the others, with 37000 and 55000 mm





252 precipitation. Comparing these derived values to other precipitation estimates allows us to provide a  
253 temporal perspective required to explain the observed EC in the pits. Other studies have shown that the  
254 annual precipitation is very altitude-level dependent in the Himalayas, and based on the altitude of the  
255 glaciers alone one would expect less than about 1000 mm in annual precipitation (Anders et al., 2006;  
256 Bookhagen and Burbank, 2010). Based on the changes in snow depth, the local precipitation was  
257 estimated using the AWS as described in section 2.2. This analysis gave a snow accumulation of about  
258 600 mm SWE in the winter season 2015-2016 and 700 mm in the 2016-2017 winter season at the  
259 location of the AWS. Over the season, a fraction of the snow evaporates or sublimates, possibly  
260 accounting for a magnitude of mm per day during favorable conditions (Stigter et al., 2018). Further,  
261 Mimeau et al. (2019) estimated the sublimation between 12 and 15 % of the total annual precipitation  
262 in the Khumbu valley, Nepal. This amount might be missed by this method using daily data.  
263 Nonetheless, our two precipitation estimates are below the observed annual precipitation of 976 mm in  
264 2012/2013 at 3950 m altitude, about 250 km to the north-west next to the Chhota Shigri glacier front  
265 (Azam et al., 2016). Measured with an automatic precipitation gauge (i.e. capturing all precipitation  
266 forms), the authors found that the majority of precipitation was during the winter season, and that the  
267 summer monsoon contributed with only 12 % to the annual precipitation. Based on these observation  
268 estimates, and the similarities with our Sunderdhunga AWS precipitation patterns, we estimate  
269 that about  $800 \pm 200$  mm is a characteristic annual precipitation amount close to where the pits were  
270 dug. If the precipitation amounts derived to explain the deposited EC in each pit is divided by 800 mm,  
271 the minimum number of years required to explain the EC observed in the pit is acquired. With this  
272 approach it is clear that it would require decades of precipitation to explain the EC in the melt layers in  
273 pits A and C. This is unrealistic, especially when the lower levels in pit F from the previous year is  
274 compared. Even the difference in EC amount between pits B, E, and D compared to F is much greater  
275 than can be explained from aggregating the EC accumulated by one year of precipitation in a single  
276 melt layer. This leads us to propose that EC must have been transported laterally in the surface layer  
277 during the melt period in the summer of 2016 and converged in the altitude range where the pits were  
278 dug. From Figure 1 it can be seen that the pits were dug in a complex terrain where slopes with  
279 increasing gradient are reaching up to the summit towards the southwest.

280

281 The data and analysis presented above lead us to propose that the old snow layers observed in pit F  
282 from 2015 are the same old snow layers observed for the pits dug in 2016. The EC equivalent  
283 precipitation profile of pit F presented in Figure 4 suggests that strong melting had taken place already  
284 in summer 2015. Hence, the old snow is composed of snow from at least the season 2013-2014 (or  
285 perhaps also earlier seasons). Stratigraphy analysis for pit F presented in Svensson et al. (2018)  
286 suggested that the snow deposition represented five seasons. The amount of precipitation represented  
287 by the EC deposition (cf. Figure 4) in the old snow is about 2100 mm, which suggests that the EC was  
288 deposited over several seasons, but less than 5 seasons. Another strong melt took place in 2016, possibly



289 leading to melting all of the snow from the season 2015-2016. In addition, during the melting phase,  
290 water and snow particulates could be transported down the slopes from areas of the glacier with steep  
291 slopes. Because the steepness of the slope decreases towards the valley, this resulted in a convergence  
292 of percolated material from areas above the sampling sites. The young snow is likely part of the 2016-  
293 2017 winter season that had started to accumulate before the sampling in October 2016 was  
294 commenced. This is confirmed by AWS data that indicates intermittent snow events in October 2016.  
295 At the AWS location a seasonal snow cover was in place in December 2016.

296

### 297 3.3 Mineral dust fraction in snow

298 An initial inspection of the mineral fractional absorption on the filters did not reveal any special  
299 common pattern in concentration between the different pits, except for the melt layer samples, which  
300 appeared to have higher concentrations than the other samples. In Figure 5, the data is grouped  
301 according to the pit stratigraphy classification, and although the absolute range of MD fractions in  
302 young snow samples is very large (5 to 71 %), the quartile range is only between 32 to 48 % with a  
303 median value of 39 %. The median value for old snow is somewhat larger at 46 %, along with the range  
304 and quartiles, which are closer together, from 26 to 70 % and from 43 to 50 %, respectively. The range  
305 of values for the melt layer are consistently higher compared to the other two snow types. The median  
306 is 78 % with a range and quartiles of 48 to 95 % and 74 to 82 %, respectively. Note that from a total of  
307 95 samples only 16 are from the melt layer.

308

309 Due to the typically heavy loading of material on the filters obtained in the melt layer, those values  
310 should be taken with caution. Non-linear effects could skew the resulting light absorption fractions  
311 towards larger values since with a very heavy loading (dark filter) the contribution by remaining  
312 particles may be over-estimated. This is because the relative contribution by additional light absorbing  
313 material decreases as the amount of material increases on very dark filters. In an extreme case, black on  
314 black will not add any contribution. The larger range of values in young snow compared to old snow is  
315 possibly an effect from the geometric thickness of the sampled slabs, which are in young snow generally  
316 thinner than in old snow, and that the density of young snow is typically less than the density of old  
317 snow. This results in each of the sampled segments in young snow representing less deposition of both  
318 water and LAP and, therefore, presenting a larger variability. Nevertheless, the ensemble of data  
319 presents similar median values for both young and old snow. The median of the percentage of the  
320 mineral dust absorption  $f_D$  value for young and old snow samples together becomes 44 %. The specific  
321 absorption by minerals is expected to be orders of magnitude smaller than BC (e.g. Utry et al., 2015),  
322 and the same is expected with respect to EC. This suggests that the deposition of minerals in the snow  
323 is orders of magnitude larger than EC. If we simply scale our characteristic EC constants ( $EC_y^*$  and



324  $EC_o^*$ ), with the median of  $f_D$  and the ratio between their specific mass absorption coefficients (MAC),  
325 according to:

326

$$327 \quad \frac{f_D}{(1-f_D)} \frac{MAC_{EC}}{MAC_D} EC_c = D_c \quad (4)$$

328

329 we arrive at a mass concentration for minerals. We use a MAC for BC of  $7.5 \text{ m}^2 \text{ g}^{-1}$  (Bond and  
330 Bergstrom, 2006). The MAC for the minerals is not known and can vary significantly, but for the sake  
331 of this test we use a MAC value representative for the mineral quartz with  $0.0023 \text{ m}^2 \text{ g}^{-1}$  (Utry et al.,  
332 2015). If we use these values we arrive at a range of  $128\text{-}384 \text{ } \mu\text{g g}^{-1}$  of minerals in the snow. This is in  
333 range with previous gravimetric observations from Himalaya (e.g. Thind et al., 2019; Zhang et al.,  
334 2018).

335

#### 336 3.4 Discussion

337 Our results indicate that the contribution to light absorption by minerals can be comparable to light  
338 absorption by EC in the Sunderdhunga area at about 5 km altitude. This translates into a mass  
339 concentration ratio between EC and minerals of more than three orders of magnitude. These large ratios  
340 are typically not reported for air samples because much of the deposited minerals are likely from local  
341 sources. This supports a hypothesis of a positive climate feedback that results in a reduction of snow  
342 cover and the exposure to larger sources of minerals.

343

344 For the Tibetan plateau, Zhang et al. (2018) estimated that the retreat of the snow cover could be  
345 advanced by more than a week due to LAP in snow. In their estimates, BC accounted for most of this  
346 effect and dust advanced the melting by about one day. The BC concentration in snow used in their  
347 calculations were about one order of magnitude larger than our derived values from the profiles in the  
348 snow pits. This difference can be attributed to the significant contribution of aerosol particle dry  
349 deposition in arid regions (Wang et al., 2014), but the range of values presented in their Table 2 reveals  
350 a potential problem from sampling surface snow. Post depositional processes (e.g.  
351 sublimation/evaporation, hoar formation, snow drift) can alter the concentration at a given location  
352 relatively fast, which is less of a problem if a deeper layer of the snow pack is investigated instead of  
353 solely the surface snow. Simply taking a larger vertical slab is not sufficient as is evident from the melt  
354 layer in the present study. The melt layer in the pits can be studied to characterize the short-term  
355 seasonal surface albedo, but the aerosol concentrations cannot be directly related to the deposition. The  
356 consistency between pits and different sampling seasons in the integrated deposition profiles above and  
357 below the melt layer show the strength in the data collected from snow pits in comparison to snap-shot  
358 conditions of surface snow.

359



#### 360 4 Conclusions

361 In this study we aimed at characterizing the observed deposition of EC in the glacier snow in the  
362 Sunderdhunga valley and to estimate the contribution from minerals to LAP in the snow. The analysis  
363 illustrates that in the sampling area of Durga Kot and Bhanolti glaciers, the deposition of EC in young  
364 snow (from current winter season) is characterized by approximately  $50 \mu\text{g m}^{-2} \text{mm}^{-1}$  SWE water, which  
365 is in the range of other observations. The median fraction of light absorption caused by minerals was  
366 about 39 % (Q1=32, Q3=48). In old snow (from previous winter seasons), the deposition was  
367 characterized by about  $150 \mu\text{g m}^{-2} \text{mm}^{-1}$  SWE water. The reason for this difference can simply be due  
368 to a larger deposition in the years before sampling was conducted, or that more water had the chance to  
369 leave the snow-pack of older snow. Different from young snow, old snow have had to survive at least  
370 one summer season. The median fraction of light absorption was 46 % (Q1=43, Q3=50) by minerals in  
371 the old snow layer. Although the variability within each layer is rather large, the obtained lower median  
372 fraction for young snow is consistent with the fact that old snow is more exposed to rock surfaces free  
373 of snow during the summer season.

374

375 Between these two layers of old and young snow, a clearly visible and very dark layer was present. This  
376 layer was most likely a result of strong melting that took place in the summers of 2015 and 2016.  
377 However, the high concentration of EC found in this layer cannot simply be explained by a collapse of  
378 the snow-pack vertically, and thus it is concluded that lateral transport of LAP (including EC and  
379 minerals) took place that resulted in a convergence of material in the altitude range of the snow pits.  
380 Different from the other two layers (young and old snow), this melt layer presented large differences  
381 with respect to EC content among the different pits. The fraction of light absorption by minerals was  
382 the highest of the three layers and was about 80 % (Q1=74, Q3=82).

383

384 The profiles of EC and the mineral absorption fraction show good agreement between subsequent years  
385 and among different pits. At the same time, the topography in this mountainous region of Himalaya  
386 evidently causes great complexity with respect to the distribution of LAP in the snow surface layer  
387 during periods of strong melt. Although data is limited in spatial and temporal dimensions our results  
388 are useful for large scale radiation impact assessments of EC deposition and minerals. In small scale  
389 regional studies, however, the effects of complex topography and spatial variability should be  
390 considered separately. Future work should further study the mineral dust and its composition in the  
391 area, in order to more accurately elucidate dust role in the snow radiation scheme in this part of the  
392 Himalaya.

393



394 Data availability

395 All data are available upon request.

396

397 Author contributions

398 J. Sv, H.H, E.A., N.D., H.L., participated in the field expedition. S.T., R.H., V.S., M. L., H.L., A.H.  
399 handled project administration. Data analysis was performed by J. Sv. and J. St. Funding acquisition:  
400 A.H. Supervision M.L. and H.L. J. Sv led the writing of the manuscript with J. St., with input from all  
401 other co-authors.

402

403 Completing interests.

404 The authors declare that they have no conflict of interest.

405

406 Acknowledgements

407 This work has been supported by the Academy of Finland project: Absorbing Aerosols and Fate of  
408 Indian Glaciers (AAFIG; project number 268004), and the Academy of Finland consortium: “Novel  
409 Assessment of Black Carbon in the Eurasian Arctic: From Historical Concentrations and Sources to  
410 Future Climate Impacts” (NABCEA project number 296302). J.Svensson acknowledges support from  
411 the two Finnish foundations: Maj and Tor Nessling and Oskar Huttunen; as well as the invited scientist  
412 grant from the UGA. J. Ström is part of the Bolin Centre for Climate Research, and acknowledges the  
413 Swedish Research Council grant 2017-03758. We are thankful for Daniela Tuomala’s work with the  
414 filter analyzes, as well as the strenuous assistance given by Sherpas and mountain guides during the  
415 expeditions to the Sunderdhunga valley.



## 416 References

- 417 Anders, A. M., Roe, G. H., Hallet, B., Montgomery, D. R., Finnegan, N. J., and Putkonen, J.: Spatial  
418 patterns of precipitation and topography in the Himalaya, *Geol. Soc. Am. Special Papers*, 398, 39–53,  
419 2006.
- 420 Azam, M. F., Ramanathan, A. L., Wagnon, P., Vincent, C., Linda, A., Berthier, E., Sharma, P., Mandal,  
421 A., Angchuk, T., Singh, V. B., and Pottakkal, J. G.: Meteorological conditions, seasonal and annual  
422 mass balances of Chhota Shigri Glacier, western Himalaya, India, *Ann. Glaciol.*, 57, 328–338, doi:  
423 10.3189/2016AoS71A570, 2016.
- 424 Bond, T. C., and Bergstrom, R. W.: Light absorption by carbonaceous particles: An investigative  
425 review, *Aerosol Sci. Tech.*, 40, 27–67, doi:10.1080/02786820500421521, 2006.
- 426 Bookhagen, B. and Burbank, D. W.: Toward a complete Himalayan hydrological budget:  
427 Spatiotemporal distribution of snowmelt and rainfall and their impact on river discharge, *J. Geophys.*  
428 *Res.*, 115, F03019, doi:10.1029/2009JF001426, 2010.
- 429 Carrico, C. M., Bergin, M. H., Shrestha, A., Dibb, J. E., Gomes, L., and Harris, J.M.: The importance  
430 of carbon and mineral dust to seasonal aerosol properties in the Nepal Himalayas, *Atmos. Environ.*, 37,  
431 2811–2824, 2003.
- 432 Chow, J. C., Watson, J. G., Crow, S., Lowenthal, D. H., and Merrifield, T.: Comparison of IMPROVE  
433 and NIOSH carbon measurements, *Aerosol Sci. Tech.*, 34, 23–34, 2001.
- 434 Flanner, M. G., Zender, C. S., Randerson, J. T., and Rasch, P. J.: Present-day climate forcing and  
435 response from black carbon in snow, *J. Geophys. Res.-Atmos.*, 112, D11202,  
436 doi.org/10.1029/2006JD008003, 2007.
- 437 Gertler, C. G., Puppala, S. P., Panday, A., Stumm, D., and Shea, J.: Black carbon and the Himalayan  
438 cryosphere: A review, *Atmos. Environ.*, 125, 404–417, doi.org/10.1016/j.atmosenv.2015.08.078, 2016.
- 439 He, C., Flanner, M. G., Chen, F., Barlage, M., Liou, K.-N., Kang, S., Ming, J., and Qian, Y.: Black  
440 carbon-induced snow albedo reduction over the Tibetan Plateau: uncertainties from snow grain shape  
441 and aerosol–snow mixing state based on an updated SNICAR model, *Atmos. Chem. Phys.*, 18, 11507–  
442 11527, doi.org/10.5194/acp-18-11507-2018, 2018.
- 443 Hooda, R.K., Kivekäs, N., O’Connor, E.J., Collaud Coen, M., Pietikäinen, J.P., Vakkari, V., Backman,  
444 J., Henriksson, S.V., Asmi, E., Komppula, M., Korhonen, H., Hyvärinen, A. P., Lihavainen, H.: Driving  
445 factors of aerosol properties over the foothills of central Himalayas based on 8.5 Years continuous  
446 measurements, *J. Geophys. Res. Atmos.*, 123, doi.org/10.1029/2018JD029744, 421-13,442, 2018.
- 447 Jacobi, H.-W., Lim, S., Ménégos, M., Ginot, P., Laj, P., Bonasoni, P., Stocchi, P., Marinoni, A., and  
448 Arnaud, Y.: Black carbon in snow in the upper Himalayan Khumbu Valley, Nepal: observations and  
449 modeling of the impact on snow albedo, melting, and radiative forcing, *The Cryosphere*, 9, 1685–1699,  
450 doi.org/10.5194/tc-9-1685-2015, 2015.
- 451 Jacobson, M. Z.: Climate response of fossil fuel and biofuel soot, accounting for soot’s feedback  
452 to snow and sea ice albedo and emissivity, *J. Geophys. Res.-Atmos.*, 109, D21201,  
453 doi.org/10.1029/2004jd004945, 2004.
- 454 Kaspari, S., Painter, T. H., Gysel, M., Skiles, S. M., and Schwikowski, M.: Seasonal and elevational  
455 variations of black carbon and dust in snow and ice in the Solu-Khumbu, Nepal and estimated radiative  
456 forcings, *Atmos. Chem. Phys.*, 14, 8089–8103, doi.org/10.5194/acp-14-8089-2014, 2014.



- 457 Krecl, P., Ström, J., and Johansson, C.: Carbon content of atmospheric aerosols in a residential area  
458 during the wood combustion season in Sweden, *Atmos. Environ.*, 41, 6974–6985,  
459 doi.org/10.1016/j.atmosenv.2007.06.025, 2007.
- 460 Kopacz, M., Mauzerall, D. L., Wang, J., Leibensperger, E. M., Henze, D. K., and Singh, K.: Origin and  
461 radiative forcing of black carbon transported to the Himalayas and Tibetan Plateau, *Atmos. Chem.*  
462 *Phys.*, 11, 2837–2852, doi.org/10.5194/acp-11-2837-2011, 2011.
- 463 Li, C., Bosch, C., Kang, S., Andersson, A., Chen, P., Zhang, Q., Cong, Z., Chen, B., Qin, D., and  
464 Gustafsson, O.: Sources of black carbon to the Himalayan-Tibetan Plateau glaciers, *Nature Commun.*,  
465 7, 12574, doi.org/10.1038/ncomms12574, 2016.
- 466 Ménégoz, M., Krinner, G., Balkanski, Y., Boucher, O., Cozic, A., Lim, S., Ginot, P., Laj, P., Gallée,  
467 H., Wagnon, P., Marinoni, A., and Jacobi, H. W.: Snow cover sensitivity to black carbon deposition in  
468 the Himalayas: from atmospheric and ice core measurements to regional climate simulations, *Atmos.*  
469 *Chem. Phys.*, 14, 4237–4249, doi.org/10.5194/acp-14-4237-2014, 2014.
- 470 Mimeau, L., Esteves, M., Zin, I., Jacobi, H.-W., Brun, F., Wagnon, P., Koirala, D., and Arnaud, Y.:  
471 Quantification of different flow components in a high-altitude glacierized catchment (Dudh Koshi,  
472 Himalaya): some cryospheric-related issues, *Hydrol. Earth Syst. Sci.*, 23, 3969–3996,  
473 doi.org/10.5194/hess-23-3969-2019, 2019.
- 474 Ming, J., Du, Z., Xiao, C., Xu, X., and Zhang, D.: Darkening of the mid-Himalaya glaciers since 2000  
475 and the potential causes, *Environ. Res. Lett.*, 7, 014021, doi:10.1088/1748-25 9326/7/1/014021, 2012.
- 476 Ming, J., Xiao, C., Du, Z., and Yang, X.: An Overview of Black Carbon Deposition in High Asia  
477 Glaciers and its Impacts on Radiation Balance, *Adv. Water Resour.*, 55, 80–87, 2013.
- 478 Petzold, A., Ogren, J. A., Fiebig, M., Laj, P., Li, S.-M., Baltensperger, U., Holzer-Popp, T., Kinne, S.,  
479 Pappalardo, G., Sugimoto, N., Wehrli, C., Wiedensohler, A., and Zhang, X.-Y.: Recommendations for  
480 reporting "black carbon" measurements, *Atmos. Chem. Phys.*, 13, 8365–8379, doi.org/10.5194/acp-13-  
481 8365-2013, 2013.
- 482 Raatikainen, T., Hyvärinen, A. P., Hatakka, J., Panwar, T. S., Hooda, R. K., Sharma, V. P., and  
483 Lihavainen, H.: The effect of boundary layer dynamics on aerosol properties at the Indo-Gangetic plains  
484 and at the foothills of the Himalayas, *Atmos. Environ.*, 89, 548–555,  
485 doi.org/10.1016/j.atmosenv.2014.02.058, 2014.
- 486 Ramanathan, V. and Carmichael, G.: Global and regional climate changes due to black carbon, *Nat.*  
487 *Geosci.*, 1, 221–227, doi.org/10.1038/ngeo156, 2008.
- 488 Santra, S., Verma, S., Fujita, K., Chakraborty, I., Boucher, O., Takemura, T., Burkhart, J. F., Matt, F.,  
489 and Sharma, M.: Simulations of black carbon (BC) aerosol impact over Hindu Kush Himalayan sites:  
490 validation, sources, and implications on glacier runoff, *Atmos. Chem. Phys.*, 19, 2441–2460,  
491 doi.org/10.5194/acp-19-2441-2019, 2019.
- 492 Sarangi, C., Qian, Y., Rittger, K., Bormann, K. J., Liu, Y., Wang, H., Wan, H., Lin, G., and Painter, T.  
493 H.: Impact of light-absorbing particles on snow albedo darkening and associated radiative forcing over  
494 high-mountain Asia: high-resolution WRF-Chem modeling and new satellite observations, *Atmos.*  
495 *Chem. Phys.*, 19, 7105–7128, doi.org/10.5194/acp-19-7105-2019, 2019.
- 496 Skiles, S. M., Flanner, M., Cook, J. M., Dumont, M., and Painter, T. H.: Radiative forcing by light-  
497 absorbing particles in snow, *Nat. Clim. Change*, 8, 964–971, doi.org/10.1038/s41558-018-0296-5,  
498 2018.





- 499 Stigter, E. E., Maxime Litt, A., Jakob Steiner, F., Pleun Bonekamp, N. J., Joseph Shea, M., and  
500 Immerzeel, W. W.: The importance of snow sublimation on a himalayan glacier. *Front. Earth Sci.* 6:108,  
501 doi: 10.3389/feart.2018.00108, 2018.
- 502 Svensson, J., Ström, J., Kivekäs, N., Dkhar, N. B., Tayal, S., Sharma, V. P., Jutila, A., Backman, J.,  
503 Virkkula, A., Ruppel, M., Hyvärinen, A., Kontu, A., Hannula, H.-R., Leppäranta, M., Hooda, R. K.,  
504 Korhola, A., Asmi, E., and Lihavainen, H.: Light-absorption of dust and elemental carbon in snow in  
505 the Indian Himalayas and the Finnish Arctic, *Atmos. Meas. Tech.*, 11, 1403–1416,  
506 doi.org/10.5194/amt-11-1403-2018, 2018.
- 507 Thind, P. S., Chandel, K. K., Sharma, S. K., Mandal, T. K., and John, S.: Light-absorbing impurities in  
508 snow of the Indian Western Himalayas: impact on snow albedo, radiative forcing, and enhanced  
509 melting, *Environ. Sci. Pollut. Res. Int.*, 26, 7566–7578, doi.org/10.1007/s11356-019-04183-5, 2019.
- 510 Utry, N., Ajtai, T., Pintér, M., Tombácz, E., Illés, E., Bozóki, Z., and Szabó, G.: Mass-specific optical  
511 absorption coefficients and imaginary part of the complex refractive indices of mineral dust components  
512 measured by a multi-wavelength photoacoustic spectrometer, *Atmos. Meas. Tech.*, 8, 401–410,  
513 doi.org/10.5194/amt-8-401-2015, 2015.
- 514 Wang, Z. W., Gallet, J. C., Pedersen, C. A., Zhang, X. S., Ström, J., and Ci, Z. J.: Elemental carbon in  
515 snow at Changbai Mountain, northeastern China: concentrations, scavenging ratios, and dry deposition  
516 velocities, *Atmos. Chem. Phys.*, 14, 629–640, doi.org/10.5194/acp-14-629-2014, 2014.
- 517 Warren, S. and Wiscombe, W.: A model for the spectral albedo of snow II. Snow containing  
518 atmospheric aerosols, *J. Atmos. Sci.*, 37, 2734–2745, 1980.
- 519 Xu, B., Cao, J., Hansen, J., Yao, T., Joswiak, D.R., Wang, N., Wu, G., Wang, M., Zhao, H., Yang, W.,  
520 Liu, X., and He, J.: Black soot and the survival of Tibetan glaciers, *P. Natl. Acad. Sci. USA*, 106,  
521 22114–22118, doi.org/10.1073/pnas.0910444106, 2009.
- 522 Zhang, R., Wang, H., Qian, Y., Rasch, P. J., Easter, R. C., Ma, P.-L., Singh, B., Huang, J., and Fu, Q.:  
523 Quantifying sources, transport, deposition, and radiative forcing of black carbon over the Himalayas  
524 and Tibetan Plateau, *Atmos. Chem. Phys.*, 15, 6205–6223, doi.org/10.5194/acp-15-6205-2015, 2015.
- 525 Zhang, Y., Kang, S., Sprenger, M., Cong, Z., Gao, T., Li, C., Tao, S., Li, X., Zhong, X., Xu, M., Meng,  
526 W., Neupane, B., Qin, X., and Sillanpää, M.: Black carbon and mineral dust in snow cover on the  
527 Tibetan Plateau, *The Cryosphere*, 12, 413–431, doi.org/10.5194/tc-12-413-2018, 2018.





528 Table 1. Snow pit details from Sunderdhunga valley. Durga Kot glacier snow pits are A-B, while C-F are from Bhanolti glacier.

Snow pit ID and elevation (m a.s.l.)	Depth interval (cm)	Snow density (g cm <sup>-3</sup> )		Water equivalent (mm m <sup>-2</sup> )	TC analyzed (μg L <sup>-1</sup> )	EC (μg L <sup>-1</sup> )		EC deposition (μg m <sup>-2</sup> )	fD (%)
		Measured	Assumed			Analyzed	Reconstructed		
A, 5055	0-3	0.38		11.4	1130	-	120	1364	24.6
	3-6	0.38		11.4	238	18	-	207	29.2
	6-9	0.35		10.5	477	47	-	495	40.4
	9-12	0.37		11.1	30300	-	3125	34688	-
	12-15	0.39		11.7	1307404	-	134685	1575819	76.1
	15-20		0.50	25.0	68177	-	7034	175855	55.1
	20-25		0.50	25.0	1398	278	-	6945	47.9
	25-30		0.50	25.0	1549	147	-	3684	49.8
	30-35		0.50	25.0	1769	271	-	6787	41.9
	35-40		0.50	25.0	1466	251	-	6273	46.5
B, 5055	40-45		0.50	25.0	883	141	-	3528	44.6
	45-50		0.50	25.0	751	142	-	3553	43.1
	50-60		0.50	50.0	1090	171	-	8544	51.5
	60-70		0.50	50.0	763	88	-	4412	45.9
	0-3	0.40		12.0	1542	95	-	1143	38.3
	3-6	0.40		12.0	693	30	-	364	27.5
	6-9	0.39		11.6	31710	-	3291	38015	77.8
	9-12	0.33		9.9	69667	-	7210	71378	75.0
	12-15	0.33		9.9	3498	-	374	3699	50.6
	15-19		0.50	20.0	-	-	267	5348	49.9
19-29		0.50	50.0	1534	246	-	12319	49.8	
29-39		0.50	50.0	1295	190	-	9480	46.2	
39-49		0.50	50.0	1517	248	-	12407	52.1	



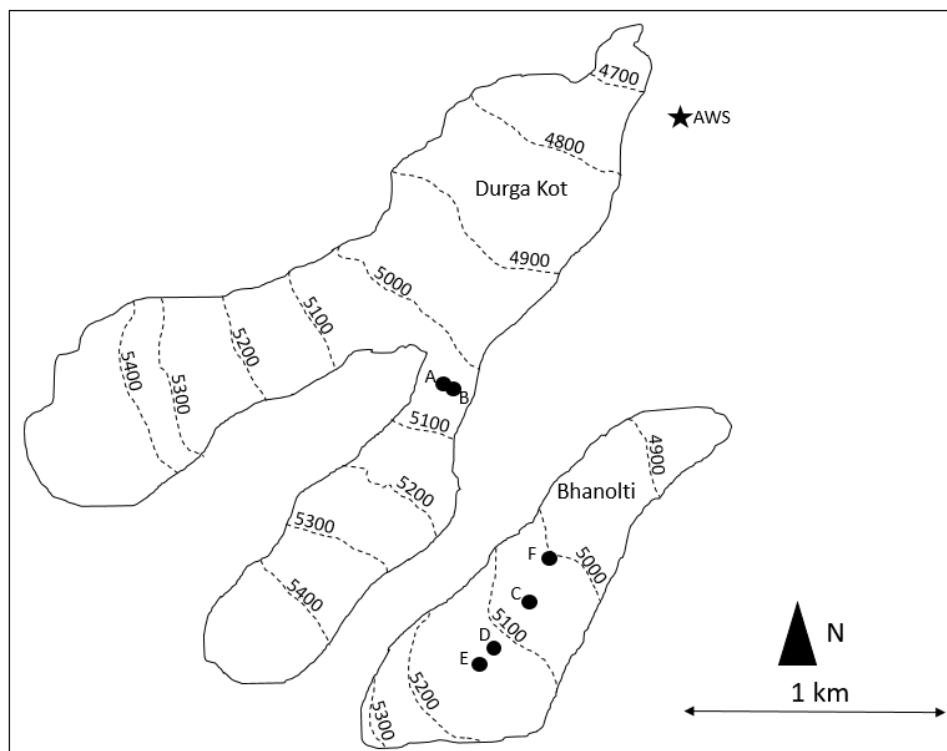
C, 5068	49-59	0.50	50.0	1753	182	-	9100	40.2
	59-69	0.50	50.0	733	103	-	5156	41.2
	69-79	0.50	50.0	730	102	-	5121	44.9
	0-3	0.40	12.0	2386	-	249	2983	47.6
	3-6	0.39	11.7	590	45	-	523	31.6
	6-11	0.39	19.5	372	34	-	658	59.4
	11-16	0.42	21.0	799	93	-	1959	54.8
	16-21	0.46	23.0	1074	141	-	3240	58.0
	21-26	0.50	25.0	1047065	-	107865	2696629	-
	26-31	0.50	25.0	4480	370	-	9257	62.0
	31-36	0.50	25.0	684	80	-	1988	58.9
	36-41	0.50	25.0	906	150	-	3746	43.6
	41-46	0.50	25.0	658	126	-	3159	44.2
	46-56	0.50	50.0	863	137	-	6871	43.5
	56-66	0.50	50.0	1191	156	-	7803	45.7
	66-76	0.50	50.0	832	144	-	7222	44.9
	76-86	0.50	50.0	802	94	-	4709	45.9
	86-96	0.50	50.0	416	51	-	2543	42.6
	96-106	0.50	50.0	609	78	-	3913	45.3
	106-116	0.50	50.0	692	76	-	3821	50.0
	116-126	0.50	50.0	500	46	-	2322	57.9
	126-136	0.50	50.0	1265	108	-	5386	59.0
D, 5125	0-3	0.39	11.7	1135	127	-	1487	35.2
	3-6	0.39	11.7	1012	91	-	1068	34.0
	6-9	0.37	11.1	449	30	-	337	42.6
	9-12	0.37	11.1	810	41	-	450	47.3
	12-15	0.37	11.0	1089	84	-	916	48.5
	15-18	0.37	11.0	357	32	-	353	38.6
	18-21	0.36	10.8	918	59	-	637	38.5
	21-24	0.42	12.6	274	23	36	448	70.8
	24-27	0.42	12.6	322	23	-	293	57.2



27-30	0.36	10.8	443	28	-	297	36.3
33-36	0.36	10.8	2393		253	2734	95.1
36-39	0.45	13.5	1714		186	2506	77.6
39-42	0.45	13.5	6806		710	9591	77.1
42-44		10.0	177424		18313	183125	-
44-49	0.50	20.0	9733		1025	20504	60.1
49-54	0.50	25.0	5708	665	-	16635	59.5
54-59	0.50	25.0	1743	232	-	5798	69.6
59-69	0.50	50.0	901	129	-	6459	46.1
E, 5143	0.33	9.9	992	128	-	1268	35.9
3-6	0.33	9.9	422	63	-	622	41.4
6-9	0.37	11.1	891	81	-	903	25.9
9-12	0.31	9.3	569	41	-	380	43.0
12-15	0.31	9.3	806	73	-	681	27.7
15-18	0.29	8.7	750	35	-	302	41.0
18-21	0.29	8.7	345	22	-	193	55.6
21-24	0.39	11.7	644		81	943	4.5
24-27	0.38	11.4	500	50	-	566	27.0
27-30	0.38	11.4	439	65	-	739	56.7
30-33	0.40	12.0	395	53	-	635	49.4
33-36	0.40	12.0	642	26	-	308	27.3
36-39	0.44	13.2	397	33	-	430	38.9
39-42	0.44	13.2	1250	53	-	705	34.8
42-45	0.44	13.2	1148	75	-	988	48.4
45-48	0.45	13.5	828	169	-	2287	81.1
48-51	0.45	13.5	901	131	-	1775	77.7
51-54	0.45	13.5	617	58	-	786	85.8
54-55	0.45	4.5	-	-	4694	21125	85.8
55-60	0.50	25.0	69606	-	7198	179946	85.8
F, 5008	0.35	10.5	4075	66		690	77.9
3-6	0.40	12.0	4821	273		3271	60.8

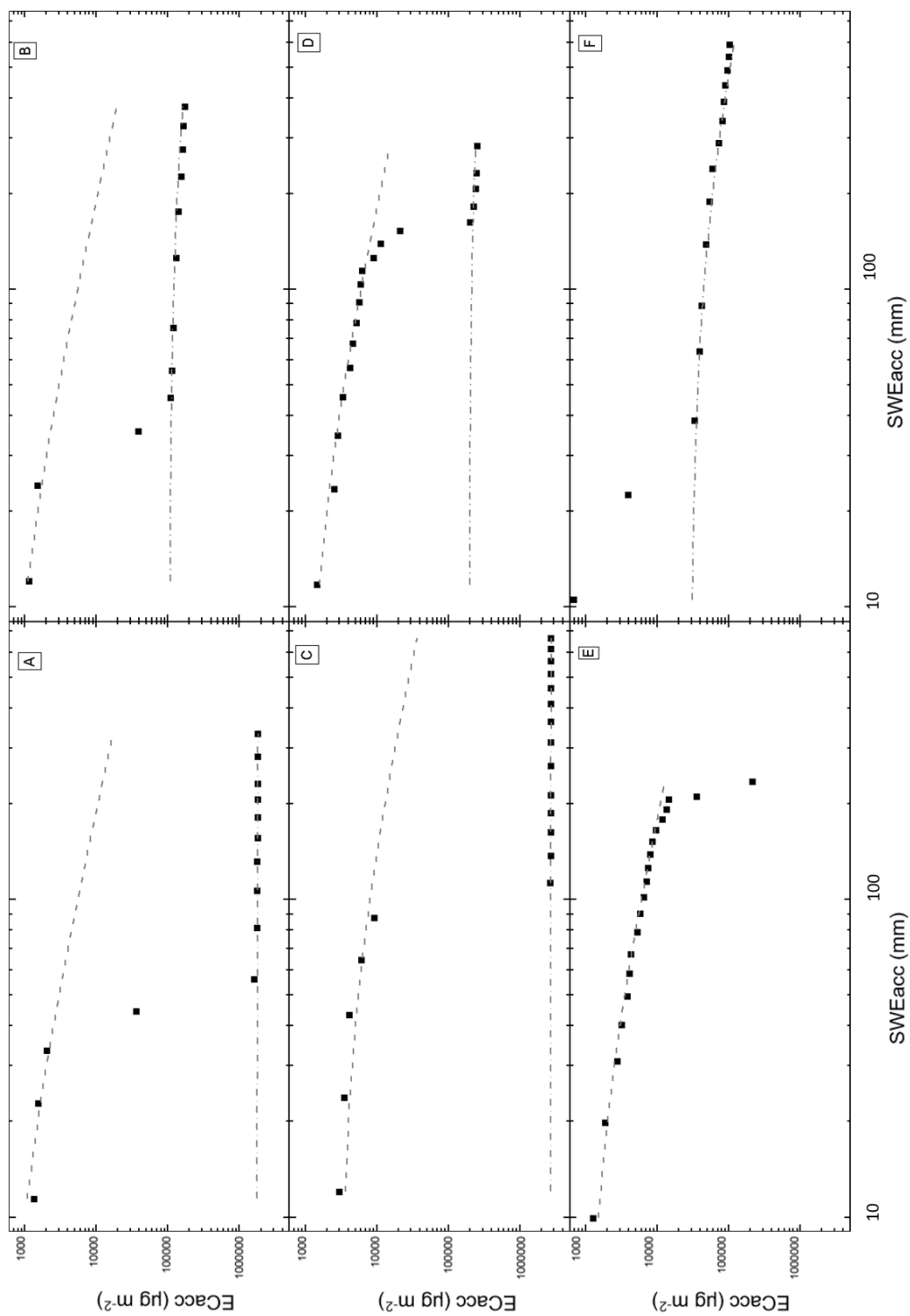


6-10	0.40	16.0	17686	233	1828	29242	69.5
10-15	0.50	25.0	3555	111		5830	60.3
15-20	0.50	25.0	859	141		2786	33.1
20-30	0.50	50.0	1324	106		7036	49.2
30-40	0.50	50.0	807	98		5278	39.6
40-50	0.50	50.0	890	270		4907	36.7
50-60	0.50	50.0	2825	179		13484	49.5
60-70	0.50	50.0	1228	93		8965	39.9
70-80	0.50	50.0	696	73		4650	36.1
80-90	0.50	50.0	483	144		3640	35.8
90-100	0.50	50.0	1190	79		7190	43.9
100-110	0.50	50.0	652	57		3965	29.5
110-120	0.50	50.0	554			2846	25.7



532

533 Figure 1. Map of glaciers with the location of the snow pits (black dots) and AWS indicated.

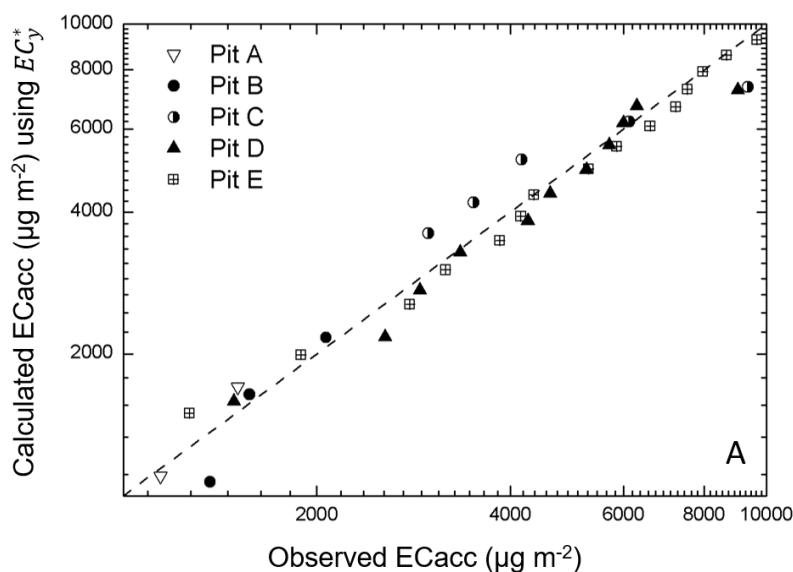




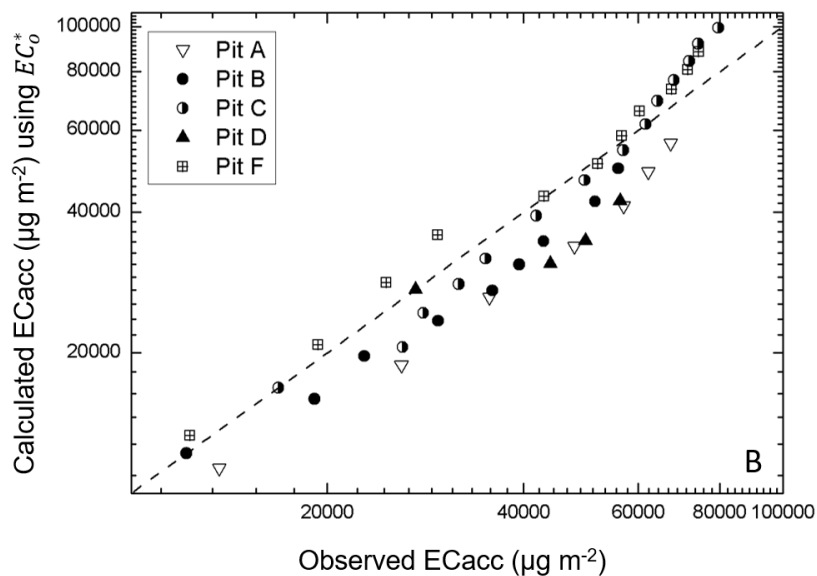
535 Figure 2. The cumulative  $\overline{EC}_i$  (ECacc) from top to bottom in the snow pits as function of accumulated  $d_{SWE}$  expressed as SWEacc (mm): (a) Pit A, (b) Pit B, (c)  
536 Pit C, (d) Pit D, (e) Pit E, (f) Pit F. The upper dashed line represents a constant deposition  $EC_y^*$  and the lower dashed-dotted line represents a constant deposition  
537  $EC_0^*$ . In pit E there were no snow samples classified as old snow, hence there is no  $EC_0^*$  line, while in in pit F there were no young snow samples, therefore no  
538  $EC_y^*$  line.



539



540



541

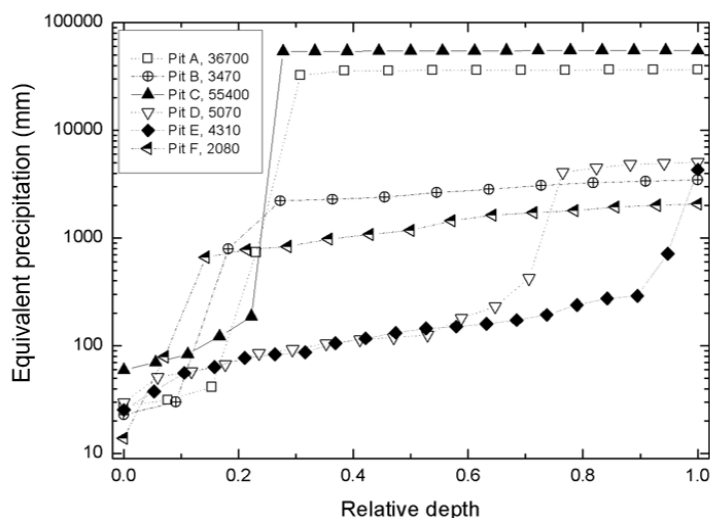
542 Figure 3. Observed and the calculated deposition using the constant deposition  $EC_y^*$  for young (a) and  
543  $EC_o^*$  for old (b) snow samples. Dashed lines indicate a 1:1 slope.

544

545

546

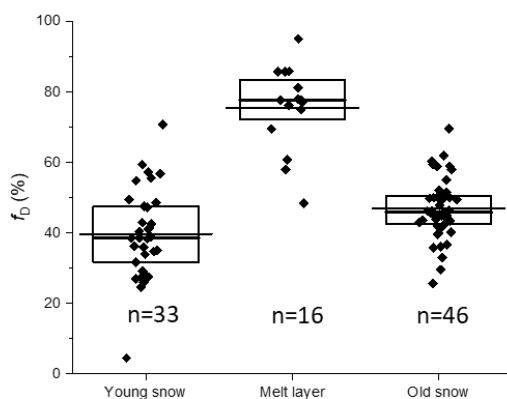




547

548 Figure 4. Equivalent precipitation for each pit based on a constant deposition  $EC_y^*$  in fresh snow as  
549 function of the relative depth of the pit from top to bottom.

550



551

552 Figure 5. Fractional dust absorption remaining after burning the filters during OC/EC analysis. The  
553 diamonds are individual values for each filter and the thin extended line represents the arithmetic  
554 average. The box and thicker line represent the quartile range and median, respectively. The number  
555 of samples are indicated in the figure as (n).